

RESEARCH

Open Access



Bioinformatics analysis reveals that CBX2 promotes enzalutamide resistance in prostate cancer

Zhu Wen^{1,2*}, Qinghua Li¹ and Guangmo Hu¹

Abstract

Enzalutamide (Enz) is commonly utilized as the initial treatment strategy for advanced prostate cancer (PCa). However, a notable subset of patients may experience resistance to Enz, resulting in reduced effectiveness. Utilizing Gene Expression Omnibus (GEO) databases, we identified CBX2 as a crucial factor in mediating resistance to Enz, primarily due to its inhibitory effect on the P53 signaling pathway. Silencing of *CBX2* using small interfering RNA (siRNA) led to elevated levels of P53 expression in LNCaP cells. This indicates that CBX2 may have a critical effect on PCa Enz resistance and could serve as a promising therapeutic target for individuals with Enz resistance.

Keywords Prostate cancer, PCa, Enzalutamide, Resistance, CBX2

Introduction

Prostate cancer (PCa) is recognized as the fifth most prevalent malignant neoplasm globally and the predominant non-cutaneous malignancy diagnosed in men, with an annual incidence exceeding 190,000 cases [1]. While localized PCa can be effectively managed through surgical intervention or radiotherapy, metastatic PCa is characterized by a poorer prognosis [2]. Androgen deprivation therapy (ADT) has been established as the conventional treatment modality for metastatic PCa [3] but about 20–30% of patients will develop castration-resistant prostate cancer (CRPC) [4]. Despite new treatments, CRPC remains incurable, so understanding its molecular drivers is crucial for developing new therapies. The dysregulation of epigenetic regulators in cancers frequently results in aberrant expression patterns that contribute to

malignant transformation [5]. Increasing evidence supports the significant involvement of epigenetics in the development and advancement of PCa through various mechanisms, such as DNA methylation, the interplay between DNA methylation and histone modification, and the regulation of non-coding RNAs [6–9]. Recent findings indicate that epigenetic perturbations orchestrated by the polycomb group (PcG) family of transcriptional repressors are crucial in the progression of PCa [10–13].

PcG proteins form two discrete complexes known as Polycomb repressive complex 1 (PRC1) and Polycomb repressive complex 2 (PRC2) [14, 15]. Within PRC1, CBX proteins from the CBX family serve as essential regulatory factors in epigenetic modification processes [16]. The human genome contains eight distinct CBX proteins (CBX1–8), each characterized by a unique N-terminal chromodomain corresponding to the Chromobox they encode at their N-terminus. PRC2 triggers transcriptional silencing by methylating H3K27 to H3K27me3 through EZH2 [17]. PRC1 complexes, including canonical and non-canonical types, contain CBX proteins (CBX2, 4, 6, 7, 8) that recognize H3K27me3 and recruit PRC1 to chromatin [18]. CBX proteins play a crucial role

*Correspondence:

Zhu Wen
urology_wen@163.com

¹ Department of Urology, The First People's Hospital of Hefei, Hefei 230061, Anhui, China

² Department of Urology, The First Affiliated Hospital of Anhui Medical University, Hefei, Anhui 230022, People's Republic of China



© The Author(s) 2024. **Open Access** This article is licensed under a Creative Commons Attribution-NonCommercial-NoDerivatives 4.0 International License, which permits any non-commercial use, sharing, distribution and reproduction in any medium or format, as long as you give appropriate credit to the original author(s) and the source, provide a link to the Creative Commons licence, and indicate if you modified the licensed material. You do not have permission under this licence to share adapted material derived from this article or parts of it. The images or other third party material in this article are included in the article's Creative Commons licence, unless indicated otherwise in a credit line to the material. If material is not included in the article's Creative Commons licence and your intended use is not permitted by statutory regulation or exceeds the permitted use, you will need to obtain permission directly from the copyright holder. To view a copy of this licence, visit <http://creativecommons.org/licenses/by-nc-nd/4.0/>.

in promoting transcriptional inhibition by recruiting PRC1 [19]. Studies have shown that CBX2 expression is linked to various tumors and is essential for male urogenital system development in individuals with XY karyotype [20]. Therefore, CBX2 may be a novel therapeutic target for advanced PCa.

Recent advancements in bioinformatic analysis have enhanced our understanding of tumor molecular mechanisms, with the choice of analysis algorithm playing a significant role. This study utilized Weighted Gene Co-expression Network Analysis (WGCNA) to identify gene modules and hub genes associated with disease, bypassing the need for differential expression gene (DEG) analysis [21, 22]. In the present investigation, *CBX2* was identified as a pivotal gene implicated in the development of resistance to Enz in PCa [23–27]. Elevated levels of CBX2 have been correlated with unfavorable prognostic outcomes in individuals affected by this disease. Our findings demonstrate that the overexpression of CBX2 hinders the P53 signaling cascade, thereby playing a role in the resistance to Enz in PCa. Consequently, CBX2 emerges as a promising candidate for therapeutic intervention in Enz-resistant patients.

Materials and methods

GEO data preprocessing and DEGs identification

The data utilized in this study were obtained from the GEO database, with specific information regarding the chosen dataset provided in Supplemental Table 1. Differential gene expression analysis was conducted to identify genes that differed between patients exhibiting sensitivity and resistance to cisplatin. Genes were classified as differentially expressed if they exhibited a \log_2 fold change (FC) greater than 1.3 and a p -value less than 0.05 in the GSE44905 [28] dataset, a \log_2 FC greater than 1.5 and a p -value less than 0.05 in the GSE104935 [29] dataset, and a \log_2 FC greater than 4 and a p -value less than 0.05 in the GSE51872 [30] dataset. Additional information can be found in the supplementary materials and methods section.

WGCNA

Utilizing the WGCNA package in the R software, common modules were clustered within atherosclerosis datasets employing a cut-off threshold of 0.25. Identification of modules exhibiting co-expression patterns with phenotypes was conducted, with supplementary details provided in the materials and methods section.

Single-cell RNA sequencing (scRNA-seq) analysis

GSE215943 [31] validated hub gene expression, excluding genes with fewer than 200 detected genes. Details are in the supplementary materials.

Cell culture and reagents

LNCaP cells were procured from the Cell Bank of Culture at the Chinese Academy of Sciences and cultured under standard conditions of 5% CO₂ and 37 °C in RPMI-1640 medium. Cell transfection procedures adhered to established protocols, employing siRNAs obtained from TSINGKE (Shanghai, China) with specific sequences outlined in Supplemental Table 2. Enzalutamide was purchased from Selleck (S1250, Shanghai, China). Further details can be found in the supplementary materials and methods section.

Western blotting

Cell lysis was performed using RIPA buffer supplemented with phosphatase and protease inhibitors, followed by protein separation via electrophoresis and subsequent transfer onto PVDF membranes. A comprehensive list of primary antibodies utilized in the study, along with their respective dilutions and sources from vendors, can be found in Supplemental Table 3. Further details can be accessed in the supplementary materials and methods section.

Colony formation assay

Cells were seeded at a density of 1×10^4 cells per well in 6-cm dishes and subsequently incubated in either 1640 medium alone or medium supplemented with 10 μ M enzalutamide for a duration of 14 days. Following the incubation period, the cells were fixed with 4% paraformaldehyde and stained with a 1% crystal violet solution for 20 min. Colony formation was quantified using ImageJ software.

Statistics

A two-tailed independent Student's t -test was conducted to evaluate statistical significance, with significance levels set at $p < 0.05$, and non-significance denoted by n.s.

Results

Identification of key Enz-resistant genes in PCa based on RNA-seq data

To identify potential target genes linked to resistance to Enz in prostate cancer, a search was carried out in the GEO database to identify genes resistant to Enz for further comprehensive analysis. A comparison of gene expression levels was conducted between LNCaP cells treated with Enz and the control group from the GSE44905 dataset, resulting in the identification of 954 upregulated DEGs and 728 downregulated DEGs that met the criteria of \log_2 FC > 1.3 and $p < 0.05$ (Fig. 1A). The study conducted a comparative analysis of gene

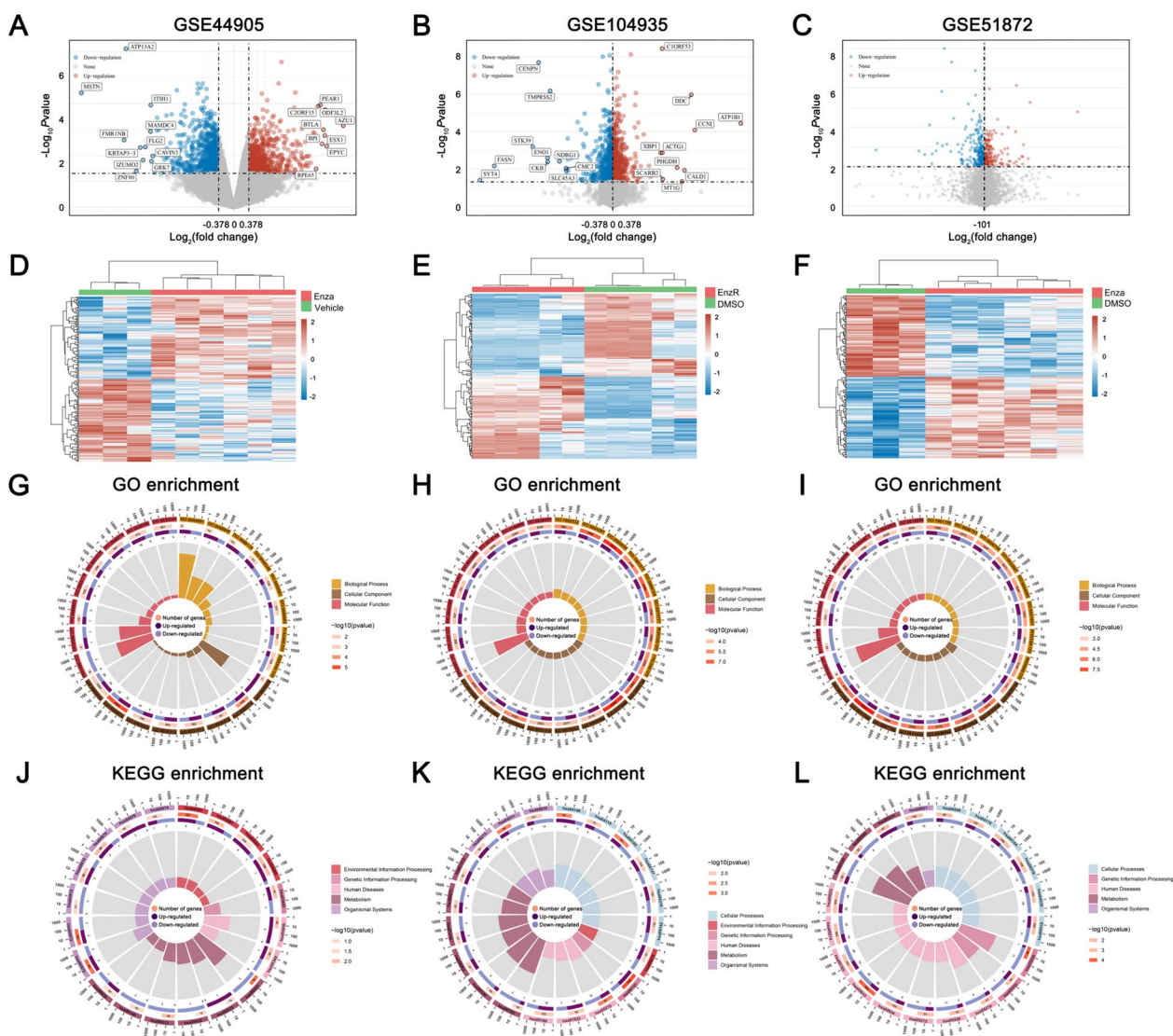


Fig. 1 Enz resistance-related genes identification. **A** Volcano plots of the DEGs in GSE44905. Red dots indicate upregulated genes; blue dots indicate downregulated genes. **B** Volcano plots of the DEGs in GSE104935. Red dots indicate upregulated genes; blue dots indicate downregulated genes. **C** Volcano plots of the DEGs in GSE51872. Red dots indicate upregulated genes; blue dots indicate downregulated genes. **D** Heatmap showing DEGs in different samples in GSE44905. **E** Heatmap showing DEGs in different samples in GSE104935. **F** Heatmap showing DEGs in different samples in GSE51872. **G** Circular enrichment of GO pathways among GSE44905 DEGs. **H** Circular enrichment of GO pathways among GSE104935 DEGs. **I** Circular enrichment of GO pathways among GSE51872 DEGs. **J** Circular enrichment of KEGG pathways among GSE44905 DEGs. **K** Circular enrichment of KEGG pathways among GSE104935 DEGs. **L** Circular enrichment of KEGG pathways among GSE51872 DEGs

expression levels in Enz-resistant LNCaP cells and Control LNCaP cells using data from the GSE104935 dataset, identifying 1121 upregulated and 859 downregulated DEGs meeting the criteria of \log_2 FC greater than 1.5 and p -value less than 0.05 (Fig. 1B). Furthermore, a comparative analysis was conducted on VCaP cells treated with Enz and the control group from the GSE51872 dataset, identifying a total of 962 upregulated and 771 downregulated DEGs that met the specified criteria of a \log_2 FC greater than 4 and a p -value

less than 0.01 (Fig. 1C). The heatmaps visually represented the clustering of these DEGs (Fig. 1D–F).

To clarify the biological characteristics linked to the emergence of Enz resistance, distinct analyses were conducted on the overexpressed DEGs in the cohorts treated with Enz and those displaying resistance to Enz, employing GO and KEGG pathway analysis. The predominant GO terms related to the reaction to Enz are depicted in Fig. 1G–I. DEGs in LNCaP and VCaP cells subjected to Enz treatment (GSE44905, GSE51872), as well as

in Enz-resistant LNCaP cells (GSE104925), exhibited enrichment in pathways linked to cellular homeostasis, mitotic DNA replication, lipid oxidation, and regulation of apoptotic signaling pathways, suggesting a potential role in regulating drug resistance in PCa. Additionally, the primary KEGG terms associated with Enz response are depicted in Fig. 1J–L. The DEGs were mainly associated with key signaling pathways like PI3K–Akt, NF-kappa B, and P53, consistent with GO enrichment analysis. This emphasizes the importance of studying molecular mechanisms to improve understanding and treatment of Enz-resistant PCa.

Enz-resistant gene co-expression networks determined by WGCNA

DEGs were primarily focused on the most significantly regulated genes, potentially neglecting others. This study utilized WGCNA to construct gene co-expression modules to investigate key gene modules and potential mechanisms associated with Enz resistance. Hierarchical clustering was employed to create color-coded modules for the cluster dendrogram, with heatmaps presented in Fig. 2A (GSE44905), Fig. 2B (GSE104935), and Fig. 2C (GSE51872). The blue module exhibited the strongest positive correlation with the Enz response trait in GSE44905 (corresponding correlation, $CC=0.92$, $p=4e-04$), as depicted in Fig. 2D. Additionally, the magenta module demonstrated a significant positive correlation with the Enz resistance trait in GSE104935 ($CC=0.87$, $p=0.001$), while another green module exhibited the strongest positive correlation with the Enz response trait in GSE51872 ($CC=0.98$, $p=4e-06$), as depicted in Fig. 2E, F.

To elucidate the crucial genes involved in the development of resistance to Enz, an effort was made to identify

shared hub genes among DEGs and hub genes derived from WGCNA modules. This investigation resulted in the identification of 79 genes in GSE44905, 42 genes in GSE104935, and 91 genes in GSE51872. Subsequently, an enrichment analysis was conducted on the common hub genes identified from the three GEO datasets using Metascape (<https://metascape.org/>). The primary Metascape terms identified in GSE44905 included the regulation of the G protein-coupled receptor signaling pathway and positive regulation of the MAPK cascade. Furthermore, the principal GO enrichment outcomes of GSE104935 comprised the immune response-regulating signaling pathway and lysosomal transport. Additionally, the top terms of GSE51872 identified through GO analysis included response to steroid hormone, PID HIF1 TFPATHWAY, and regulation of chemokine production.

Expression and prognosis of hub genes in PCa

To inform clinical decision-making and stratify Enz-resistant conditions, it is essential that the information obtained from Enz-resistant samples remains consistent. Consequently, a comparative analysis was performed on hub genes identified in three GEO datasets, revealing that *CBX2*, *DCAF6*, *FAM117B*, and *TMEM141* were consistently identified across all three datasets (Fig. 3A). The mRNA expression levels of these four candidate genes in TCGA dataset are depicted in Fig. 3B. Consequently, *CBX2* demonstrates elevated expression levels in PCa samples and is notably associated with the prognostic outcomes of PCa patients as indicated by Kaplan–Meier survival analysis (Fig. 3C). Moreover, among the four genes identified through Venn diagram analysis, *CBX2* displays statistically significant differences between the control and Enz-treated LNCaP groups (Fig. 3D–E), as well as between the control and Enz-resistant VCaP

(See figure on next page.)

Fig. 2 WGCNA reveals Enz-resistant gene co-expression networks. **A** WGCNA analysis of Enz response samples in GSE44905. The dendrogram represented the clusters of differentially expressed genes based on different metrics. Each branch represented one gene, and each color below the branches represented one co-expression module. **B** WGCNA analysis of Enz resistance samples in GSE104935. The dendrogram represented the clusters of differentially expressed genes based on different metrics. Each branch represented one gene, and each color below the branches represented one co-expression module. **C** WGCNA analysis of Enz resistance samples in GSE51872. The dendrogram represented the clusters of differentially expressed genes based on different metrics. Each branch represented one gene, and each color below the branches represented one co-expression module. **D** The heatmap showed the correlation between gene modules and Enz response. The correlation coefficient in each cube represented the correlation between gene modules and traits, which decreased from red to blue. **E** The heatmap showed the correlation between gene modules and Enz resistance. The correlation coefficient in each cube represented the correlation between gene modules and traits, which decreased from red to blue. **F** The heatmap showed the correlation between gene modules and Enz resistance. The correlation coefficient in each cube represented the correlation between gene modules and traits, which decreased from red to blue. **G** The common hub genes shared between DEGs and WGCNA derived from GSE44905 were visualized in a Venn diagram. **H** The common hub genes shared between DEGs and WGCNA derived from GSE104935 were visualized in a Venn diagram. **I** The common hub genes shared between DEGs and WGCNA derived from GSE51872 were visualized in a Venn diagram. **J** The top enriched GO pathways among common hub genes from the GSE44905. The horizontal axis represented the p -value of GO terms on Metascape. **K** The top enriched GO pathways among common hub genes from the GSE104935. The horizontal axis represented the p -value of GO terms on Metascape. **L** The top enriched GO pathways among common hub genes from the GSE51872. The horizontal axis represented the p -value of GO terms on Metascape

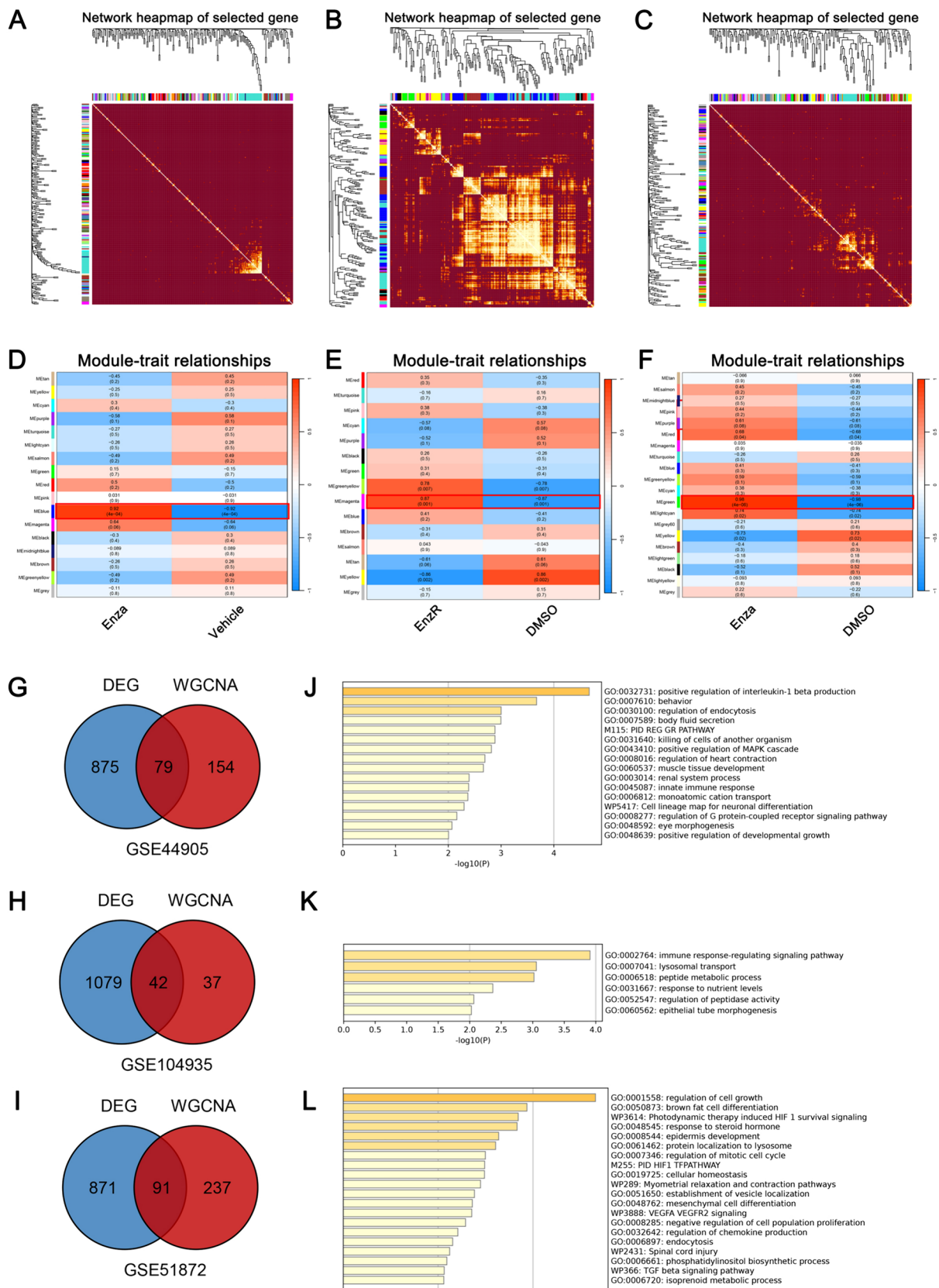


Fig. 2 (See legend on previous page.)

groups (Fig. 3F). Taken together, these findings suggest that *CBX2* may serve as a promising biomarker for Enz resistance in PCa.

CBX2-related downstream signaling pathways identification

After establishing *CBX2*'s involvement in Enz resistance in PCa, our objective was to investigate the molecular mechanisms underlying *CBX2*'s pro-resistance role in PCa through gene expression analysis of scRNA-seq data from a variety of PCa samples. Subsequently, gene expression profiles were extracted from two Enz-treated samples and one control sample within the GSE215943 dataset. Following appropriate sequencing depth adjustment, gene count detection, and data normalization steps, a subset of 2000 genes showing significant variability was chosen for subsequent analysis. Subsequently, after the application of quality control filters, a total of 31,312 cells were analyzed, each containing a median of 24,371 genes per cell.

The dimensionality reduction procedure was executed utilizing the "RunPCA" function, leading to the discernment of 12 clusters at a resolution of 0.5 (Fig. 4A, B). Next, an evaluation of the distribution of these cellular clusters across the two sample types was conducted and depicted (Fig. 4C). The heatmap exhibited the top 5 genes displaying notable variability within each cluster (Fig. 4D). Following this, a comprehensive analysis of the visualization outputs generated by CellChat was undertaken for various analytical objectives. The hierarchy plot and circle plot employed distinct color schemes to depict distinct cell groups, whereas the bubble plot utilized color intensity to indicate the relative likelihood of communication (Fig. 4E, F). The results suggest that clusters 7 and 10 primarily functioned as sources, clusters 3, 5, and 6 as recipients, and clusters 0, 1, 2, 4, 8, 9, and 11 as both sources and recipients. Additionally, an investigation of the interactions among the nine clusters entailed examining interactions in which each cluster served as both a target and a source. The bidirectional interactions between outgoing and incoming signaling within these clusters involved pathways such as NOTCH, WNT, and IGF (Fig. 4G).

Prior studies have demonstrated a strong association between *CBX2* and the Notch signaling pathway in kidney renal papillary cell carcinoma [32]. To investigate

the role of *CBX2* in the development of Enz resistance in PCa, our study examined the Notch signaling pathway in cluster communications. Our findings indicate that clusters 0 and 6 serve as primary sources, while the other clusters act as main receivers. Additionally, the distribution and expression patterns of hub genes *CBX2*, *DCAF6*, *FAM117B*, and *TM3M141* are depicted in Fig. 4I, J.

Furthermore, to emphasize the predominant signaling pathway activated within each cluster, GSVA was conducted across the 12 clusters. The results indicated that in clusters 0 and 1, there is an upregulation of the *HALLMARK_INTERFERON_ALPHA_RESPONSE*. Besides, there is an upregulation of the *HALLMARK_ANDROGEN_RESPONSE* in cluster 2, and an upregulation of the *HALLMARK_PANCREAS_BETA_CELLS* in cluster 3, among others (Fig. 5A). Subsequently, the cells were categorized into *CBX2*⁺ and *CBX2*⁻ groups for the purpose of analyzing gene expression disparities. GO enrichment analysis revealed enrichment in cell survival pathways such as the cell cycle process, DNA metabolic process, and mitotic cell cycle. KEGG enrichment analysis revealed the involvement of the P53 signaling pathway, Cell cycle, and Apoptosis (Fig. 5B, C). Additionally, GSEA demonstrated the essential role of *CBX2* activity in promoting prostate cancer (PCa) cell survival by upregulating the cell cycle signaling in *CBX2*⁺ cells. Moreover, the inhibition of the P53 signaling pathway was associated with *CBX2*⁻ cells, indicating that the upregulation of *CBX2* suppresses the P53 signaling pathway, thereby contributing to enzalutamide resistance in PCa (Fig. 5D, E).

In vitro experiments validated the role of *CBX2* in Enz-response

To validate the hypothesis that Enz response can activate *CBX2* and enhance prostate cancer cell survival through modulation of the P53 signaling pathway, resulting in Enz resistance, an in vitro model of PCa was established using LNCaP cells. The expression levels of *CBX2* and P53 were assessed following treatment of LNCaP cells with Enz at a concentration of 10 μ M for a specified duration. Western blot analysis confirmed that stimulation with Enz led to downregulation of the P53 signaling pathway in LNCaP cells (Supplement Fig. A, B).

Our functional analysis indicated that the acquisition of Enz resistance is linked to alterations in the P53 signaling pathways. Collectively, the findings from our colony

(See figure on next page.)

Fig. 3 Expression and prognosis of hub genes. **A** The common hub genes shared among three GSE datasets were visualized in a Venn diagram. **B** The expression of four selected genes in the TCGA database, PCa (red) and normal (gray). **C** Kaplan–Meier curves, respectively, for disease-free survival (DFS), and of PCa patients with high versus low expression of four selected genes in TCGA. **D** Estimation of hub gene expression in GSE44905. **E** Estimation of hub gene expression in GSE104935. **F** Estimation of hub gene expression in GSE51872. * $p < 0.05$

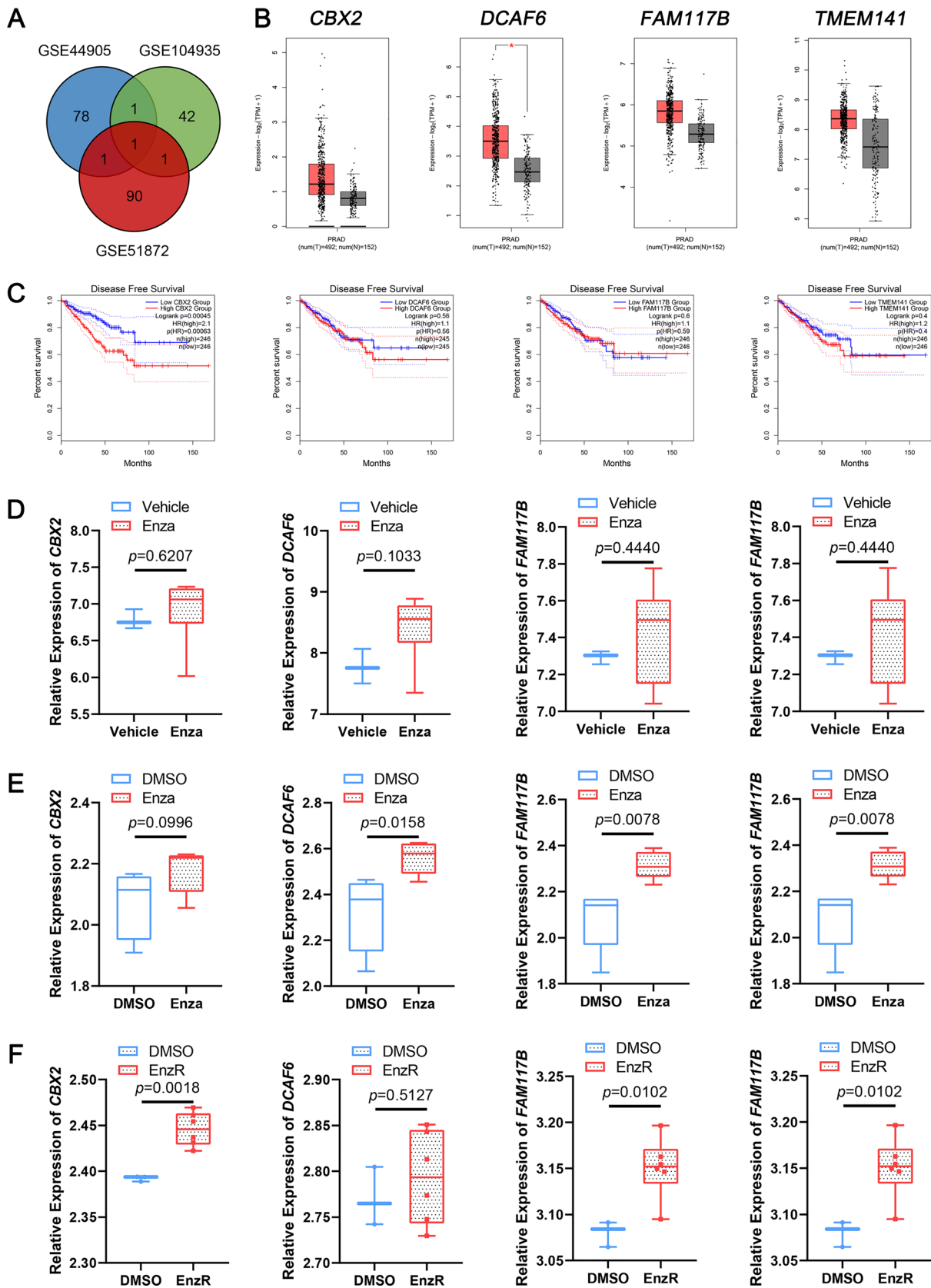


Fig. 3 (See legend on previous page.)

formation assay suggest that resistance stemming from CBX2 activation could potentially be mitigated through a combination of *CBX2* knockdown and Enz treatment (Supplement Fig. 1C, D). Consequently, we posit that the CBX2-related pathway may contribute to the development of Enz resistance. Our collective in vitro experimental results indicate that the inhibition of CBX2 may lead to the reactivation of the P53 pathway and suppression of resistance to Enz in prostate cancer. This underscores the therapeutic potential of targeting CBX2 in the treatment of advanced prostate cancer.

Discussion

A significant clinical obstacle exists in the identification of patients at risk for developing lethal resistance and disseminated PCa, as well as distinguishing those who will not progress to metastatic disease [33]. Despite extensive sequencing initiatives, only a limited number of genetic mutations are consistently observed in PCa, indicating a potential role for epigenetic modifications in disease progression [34]. Targeting epigenetic vulnerabilities to reverse chromatin alterations linked to androgen receptor signaling inhibitor resistance may enhance treatment sensitivity [35]. The integration of this strategy with endocrine therapy has the potential to induce lethality in PCa cells. Besides, additional factors like comorbidity or the specific drug used to start the ADT can influence the prognosis of prostate cancer patients. Previous studies have reported that whether hormonal therapy, especially in advanced prostate cancer, acts as a protective factor or a risk factor during COVID-19 could be useful [36]. Moreover, androgen-receptor-axis-targeted (ARAT) agents improve overall survival in metastatic CSPC and discourage their combined use with docetaxel in this setting [37]. In addition, tumor microenvironment (TME) has been claimed as one of the most important factors of prostate cancer progression since the androgen signals were reported to mutually interplay and enhance inflammation and tumorigenic activation [38], and the periprostatic adipose tissue promotes prostate cancer resistance

to docetaxel by paracrine IGF-1 upregulation of TUBB2B beta-tubulin isoform [39]. This study presents evidence of the upregulation of CBX2 in Enz-resistant PCa and its association with unfavorable clinical outcomes. Additionally, our findings reveal that depletion of CBX2 leads to cell death in PCa cells in vitro, accompanied by the reactivation of the P53 pathway, thereby inhibiting PCa progression. Taken together, these results suggest that CBX2 may serve as a potential therapeutic target in advanced PCa.

This study investigated the role of CBX2 in mediating resistance to Enz in the treatment of PCa. Various bioinformatics approaches were employed to analyze gene expression profiles of samples displaying resistance to Enz. Initial analysis of the GSE44905 dataset identified 954 upregulated DEGs and 728 downregulated DEGs in Enz-treated LNCaP cells. Similarly, the GSE104935 dataset revealed 1121 upregulated and 859 downregulated DEGs in Enz-resistant LNCaP cells, while the GSE51872 dataset showed 962 upregulated and 771 downregulated DEGs in Enz-treated VCaP cells. Furthermore, the WGCNA is widely recognized as a more effective method for identifying internal functional modules among important genes in comparison to DEG analysis [40–42]. However, there is a gap in the literature regarding the utilization of WGCNA in investigating Enz resistance in PCa [43]. In the examination of three GEO datasets, several key gene modules were identified as significant contributors to the response to Enz. By conducting a thorough analysis of both DEGs and WGCNA, the crucial gene *CBX2* was pinpointed and subsequently validated through scRNA-seq analysis and in vitro experiments. The inhibition of *CBX2* has been shown to reactivate the P53 pathway in prostate cancer cells, providing insight into the mechanisms involved in enzalutamide resistance in prostate cancer.

Previous research has demonstrated that CBX2 can influence chromatin accessibility through the MAPK pathway in acute myeloid leukemia [44]. Additionally, earlier studies have indicated that p38 MAPK plays

(See figure on next page.)

Fig. 4 scRNA-seq data validated the selected hub genes. **A** The UMAP was utilized to partition cells into 12 distinct clusters, with each cluster being represented by a unique color that corresponded to its numbered phenotype. **B** The UMAP was used to partition cells according to different sample types. **C** The distribution of cell proportions across distinct groups is depicted on a graph, where the vertical axis denotes the proportion of each cell cluster. **D** The heatmap presents the expression of the top 5 DEGs (rows) in each cell cluster (column). **E** Cell–cell communication signaling network among the 9 clusters analyzed with CellChat. The right panel showed that cell clusters were located based on the count of their significant incoming (Y-axis) or outgoing (X-axis) signaling pattern. **F** Number of interactions in 12 cell clusters. The width of the lines indicates the number of pairs. Different colors represent different signal sources. **G** Heatmap of the CellChat signaling in each cluster. The left panel shows the outgoing signaling patterns (expression weight value of signaling molecules) and the right panel shows the incoming signaling patterns (expression weight value of signaling receptors). A gradient of white to dark green indicates a low to high expression weight value in the heatmap. **H** The inferred NOTCH2 signaling pathway network. **I** Feature plots showing the distribution of *CBX2*, *DCAF6*, *FAM117B*, and *TMEM141* in 12 cell clusters. **J** Violin plots showing the distribution of indicated genes in various cell clusters

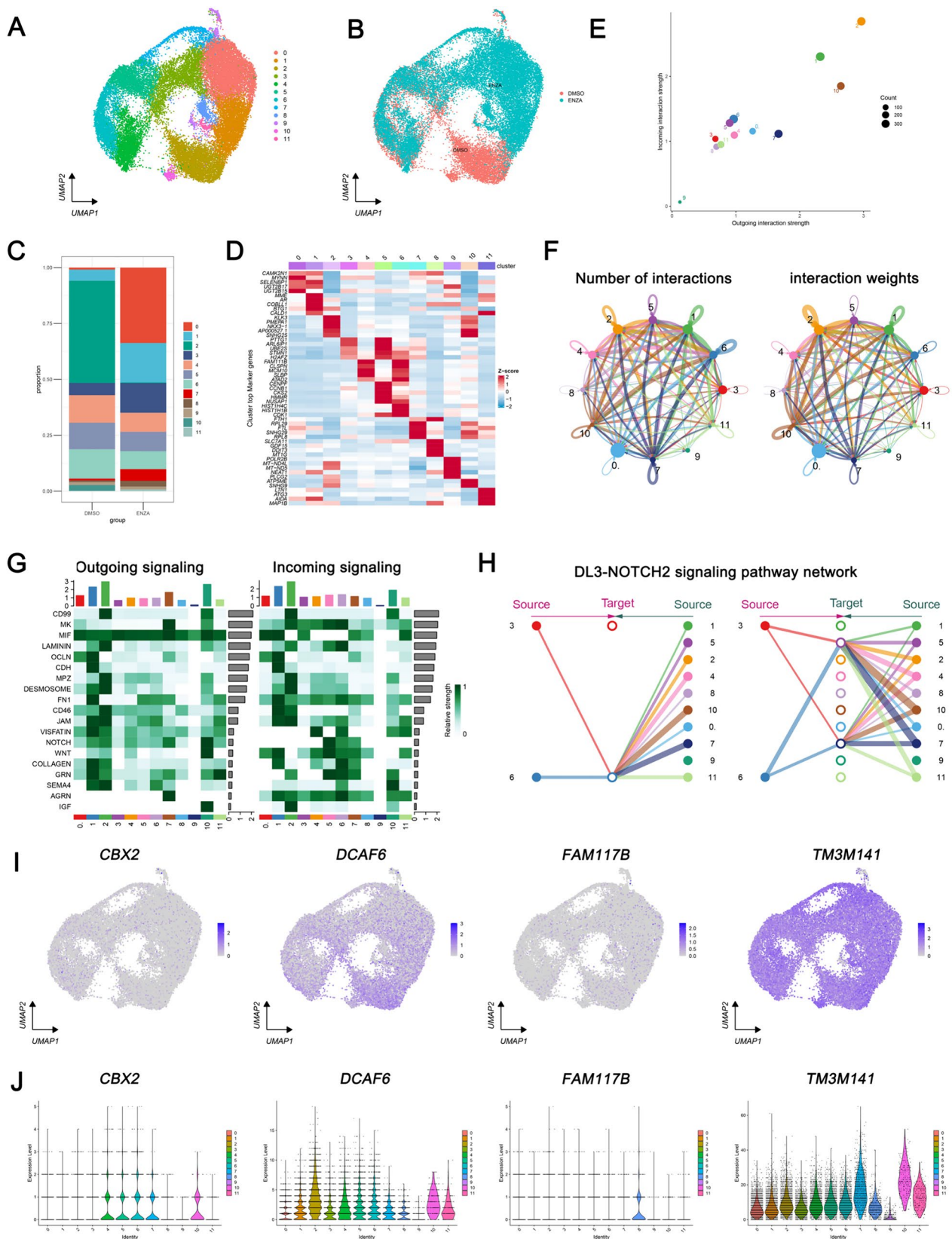


Fig. 4 (See legend on previous page.)

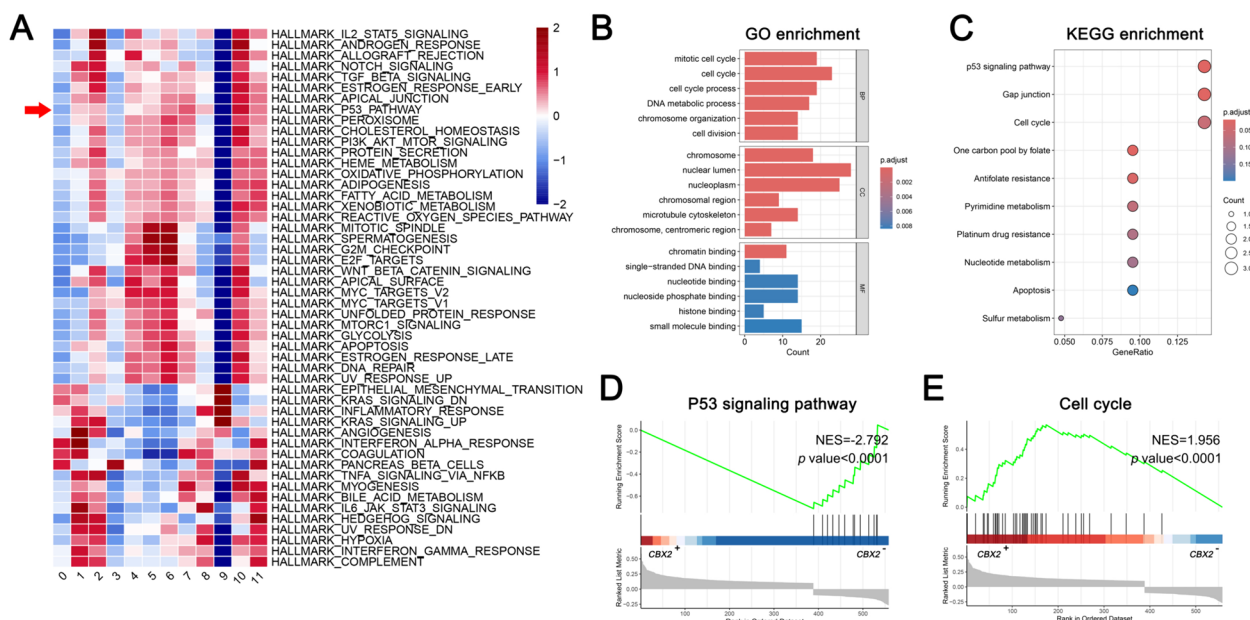


Fig. 5 In vitro experiments validated the role of CBX2 in Enz-response. **A** Heatmap showing different pathways enriched in the 12 cell clusters by GSEA. Each column represents different groups or subpopulations of cells, and each row represents a pathway. The redder the color, the higher the score, and the bluer the color, the lower the score. **B** The top enriched GO pathways among DEGs of *CBX2*⁺ and *CBX2*⁻ cells were identified and presented in a graphical representation. **C** The top enriched KEGG pathways among DEGs of *CBX2*⁺ and *CBX2*⁻ cells were identified and presented in a graphical representation. **D** The P53 signaling pathway was identified and presented in a graphical representation by GSEA. **E** The cell cycle pathway was identified and presented in a graphical representation by GSEA

a role in promoting metastasis and invasion, and that p38 activity is essential for maintaining colorectal cancer cell metabolism [45]. Hence, it is posited that the removal of CBX2 may impact cancer cell proliferation by modulating the MAPK signaling pathway. Furthermore, recent research has demonstrated that CBX2 is notably overexpressed among various models of metastatic and castration-resistant PCa, underscoring the essential function of the PcG family of epigenetic regulators in PCa cell survival and metastasis [46]. Our results suggest that the CBX2-related mechanism could play a crucial role in the emergence of resistance to Enzalutamide. To delve deeper into this correlation, we utilized siRNA to suppress the expression of the *CBX2* gene in Enz-treated LNCaP cells and assessed its impact on the activation of the P53 pathway.

Despite the rigorous analyses and extensive experimental validation conducted in our study, it is important to acknowledge certain limitations. Specifically, the intricate nature of tissues and living organisms may result in cellular-level analyses not always offering a comprehensive representation of the organism. Additionally, additional in vitro and in vivo studies are necessary to verify the reciprocal impact of CBX2 on Enz

resistance. It is important to highlight that the absence of RNA-seq data from Enz-resistant patient tissues poses a constraint in this research.

Conclusion

This research employed integrated bioinformatics analysis to investigate the potential mechanisms associated with resistance to Enz, revealing the hub gene *CBX2* as a potential pivotal regulatory factor. Subsequent in vitro experiments conducted on LNCaP cells treated with Enz confirmed the significance of CBX2, particularly in the context of the CBX2/P53 axis. These results provide novel insights into the mechanisms underlying resistance to Enz.

Abbreviations

GEO	Gene Expression Omnibus
siRNA	Small interfering RNA
PCa	Prostate cancer
CRPC	Castration-resistant prostate cancer
WGCNA	Weighted gene co-expression network analysis
DEG	Differential expression gene
scRNA-seq	Single-cell RNA sequencing
GO	Gene Ontology
KEGG	Kyoto Encyclopedia of Genes and Genomics
TCGA	The Cancer Genome Atlas

Supplementary Information

The online version contains supplementary material available at <https://doi.org/10.1186/s40001-024-02021-0>.

Supplementary Material 1: Supplement Fig. 1A Analysis of the CBX2 and P53 relative protein levels in LNCaP cell lines by Western blotting. Quantitative analysis of the Western blotting results by Image J software. Colony formation assay of LNCaP cells after 14 days of 10 μ M Enz treatment. Quantitative analysis of the Colony formation assay by Image J software. Error bars, \pm SD. * $p < 0.05$, ** $p < 0.01$, *** $p < 0.001$, **** $p < 0.0001$, ns, not significant. Supplement Table 1. GEO Datasets used. Supplement Table 2. siRNA list. Supplement Table 3. Antibody list.

Acknowledgements

We express our gratitude to all the individuals who took part in this research.

Author contributions

Z Wen contributed to the conception and design of the manuscript. Z Wen contributed to the acquisition of data. Z Wen contributed to the manuscript writing. Q Li and G Hu contributed to the data management and analysis.

Funding

The present research was funded by National Natural Science Foundation of China (82071637).

Data availability

The datasets utilized in this study are accessible through online repositories. The authors of this article will provide the raw data that underpin their findings, without any unwarranted hesitation.

Declarations

Ethics approval and consent to participate

All procedures performed in this study were in accordance with the ethical standards of the Ethics Committee of The First People's Hospital of Hefei and with the 1964 Helsinki Declaration and its later amendments or comparable ethical standards.

Competing interests

There are no potential conflicts of interest.

Received: 13 June 2024 Accepted: 9 August 2024

Published online: 22 August 2024

References

- Siegel RL, Giaquinto AN, Jemal A. Cancer statistics, 2024. *CA Cancer J Clin*. 2024;74:12–49.
- Qiu H, Cao S, Xu R. Cancer incidence, mortality, and burden in China: a time-trend analysis and comparison with the United States and United Kingdom based on the global epidemiological data released in 2020. *Cancer Commun (Lond)*. 2021;41:1037–48.
- Cheng Q, et al. Pre-existing castration-resistant prostate cancer-like cells in primary prostate cancer promote resistance to hormonal therapy. *Eur Urol*. 2022;81:446–55.
- Schaeffer EM, et al. Prostate cancer, version 4.2023, NCCN Clinical Practice Guidelines in Oncology. *J Natl Compr Canc Netw*. 2023;21:1067–96.
- Ge R, et al. Epigenetic modulations and lineage plasticity in advanced prostate cancer. *Ann Oncol*. 2020;31:470–9.
- Franceschini GM, et al. Noninvasive detection of neuroendocrine prostate cancer through targeted cell-free DNA methylation. *Cancer Discov*. 2024;14:424–45.
- Zhang M, et al. P300/SP1 complex mediating elevated METTL1 regulates CDK14 mRNA stability via internal m7G modification in CRPC. *J Exp Clin Cancer Res*. 2023;42:215.
- Beltran H, et al. Divergent clonal evolution of castration-resistant neuroendocrine prostate cancer. *Nat Med*. 2016;22:298–305.
- Chen H, et al. Non-drug efflux function of ABCG5 promotes enzalutamide resistance in castration-resistant prostate cancer via upregulation of P65/AR-V7. *Cell Death Discov*. 2022;8:241.
- Clermont PL, et al. Identification of the epigenetic reader CBX2 as a potential drug target in advanced prostate cancer. *Clin Epigenetics*. 2016;8:16.
- Crea F, Clermont PL, Mai A, Helgason CD. Histone modifications, stem cells and prostate cancer. *Curr Pharm Des*. 2014;20:1687–97.
- Hasan S, et al. Proton therapy for high-risk prostate cancer: results from the Proton Collaborative Group PCG 001-09 prospective registry trial. *Prostate*. 2023;83:850–6.
- Park SH, et al. Going beyond Polycomb: EZH2 functions in prostate cancer. *Oncogene*. 2021;40:5788–98.
- Khan AA, Lee AJ, Roh TY. Polycomb group protein-mediated histone modifications during cell differentiation. *Epigenomics*. 2015;7:75–84.
- Su W, et al. The polycomb repressor complex 1 drives double-negative prostate cancer metastasis by coordinating stemness and immune suppression. *Cancer Cell*. 2019;36:139–155.e110.
- Grimaldi AM, Affinito O, Salvatore M, Franzese M. CBX family members in two major subtypes of renal cell carcinoma: a comparative bioinformatic analysis. *Diagnostics (Basel)*. 2022;12:2452.
- Laugesen A, Højfeldt JW, Helin K. Molecular mechanisms directing PRC2 recruitment and H3K27 Methylation. *Mol Cell*. 2019;74:8–18.
- Li J, Dallmayer M, Kirchner T, Musa J, Grünewald TGP. PRC1: linking cytokinesis, chromosomal instability, and cancer evolution. *Trends Cancer*. 2018;4:59–73.
- Gao Z, et al. PCGF homologs, CBX proteins, and RYBP define functionally distinct PRC1 family complexes. *Mol Cell*. 2012;45:344–56.
- Naqvi AAT, Rizvi SAM, Hassan MI. Pan-cancer analysis of Chromobox (CBX) genes for prognostic significance and cancer classification. *Biochim Biophys Acta Mol Basis Dis*. 2023;1869: 166561.
- Langfelder P, Horvath S. WGCNA: an R package for weighted correlation network analysis. *BMC Bioinformatics*. 2008;9:559.
- Han J, et al. Intratumoral immune heterogeneity of prostate cancer characterized by typing and hub genes. *J Cell Mol Med*. 2023;27:101–12.
- Clermont PL. Epigenetics-based diagnostic and therapeutic strategies: shifting the paradigm in prostate cancer. *Epigenomics*. 2023;15:75–87.
- Xu X et al. The predictive significance of chromobox family members in prostate cancer in humans. *Cell Oncol (Dordr)* 2024.
- Mather RL, et al. The evolutionarily conserved long non-coding RNA LINC00261 drives neuroendocrine prostate cancer proliferation and metastasis via distinct nuclear and cytoplasmic mechanisms. *Mol Oncol*. 2021;15:1921–41.
- Lercher L, et al. Identification of two non-peptidergic small molecule inhibitors of CBX2 binding to K27 trimethylated oligonucleosomes. *SLAS Discov*. 2022;27:306–13.
- Wang W, et al. LncRNA PCAT6 promotes the proliferation, migration and invasion of pancreatic ductal adenocarcinoma via regulating miR-185-5p/CBX2 axis. *Pathol Res Pract*. 2020;216: 153074.
- Guerrero J, Alfaro IE, Gómez F, Protter AA, Bernales S. Enzalutamide, an androgen receptor signaling inhibitor, induces tumor regression in a mouse model of castration-resistant prostate cancer. *Prostate*. 2013;73:1291–305.
- Li S, et al. Activation of MAPK signaling by CXCR7 leads to enzalutamide resistance in prostate cancer. *Cancer Res*. 2019;79:2580–92.
- Arora VK, et al. Glucocorticoid receptor confers resistance to antiandrogens by bypassing androgen receptor blockade. *Cell*. 2013;155:1309–22.
- Asberry AM, et al. Reprogramming landscape highlighted by dynamic transcriptomes in therapy-induced neuroendocrine differentiation. *Comput Struct Biotechnol J*. 2022;20:5873–85.
- Liu Y, et al. Identification of prognostic stemness-related genes in kidney renal papillary cell carcinoma. *BMC Med Genomics*. 2024;17:121.
- Chen H, et al. The modified prostate health index (PHI) outperforms PHI density in the detection of clinical prostate cancer within the PSA grey zone. *Int Urol Nephrol*. 2022;54:749–56.
- Shangguan X, et al. Squalene epoxidase metabolic dependency is a targetable vulnerability in castration-resistant prostate cancer. *Cancer Res*. 2022;82:3032–44.

35. Chen H, et al. CRISPR genome-wide screening identifies PAK1 as a critical driver of ARSI cross-resistance in prostate cancer progression. *Cancer Lett.* 2024;587: 216725.
36. Di Lorenzo G, et al. Clinical characteristics of metastatic prostate cancer patients infected with COVID-19 in South Italy. *Oncology.* 2020;98:743–7.
37. Buonerba C, et al. Predictors of efficacy of androgen-receptor-axis-targeted therapies in patients with metastatic castration-sensitive prostate cancer: a systematic review and meta-analysis. *Crit Rev Oncol Hematol.* 2020;151: 102992.
38. Miro C, et al. Thyroid hormone and androgen signals mutually interplay and enhance inflammation and tumorigenic activation of tumor micro-environment in prostate cancer. *Cancer Lett.* 2022;532: 215581.
39. Liotti A, et al. Periprostatic adipose tissue promotes prostate cancer resistance to docetaxel by paracrine IGF-1 upregulation of TUBB2B beta-tubulin isoform. *Prostate.* 2021;81:407–17.
40. Rezaei Z, et al. Identification of early diagnostic biomarkers via WGCNA in gastric cancer. *Biomed Pharmacother.* 2022;145: 112477.
41. Luo Z, et al. Pan-cancer analysis identifies telomerase-associated signatures and cancer subtypes. *Mol Cancer.* 2019;18:106.
42. Song D, et al. Identification of the receptor of oncolytic virus M1 as a therapeutic predictor for multiple solid tumors. *Signal Transduct Target Ther.* 2022;7:100.
43. Zhang H, et al. The molecular feature of macrophages in tumor immune microenvironment of glioma patients. *Comput Struct Biotechnol J.* 2021;19:4603–18.
44. Del Gaudio N, et al. CBX2 shapes chromatin accessibility promoting AML via p38 MAPK signaling pathway. *Mol Cancer.* 2022;21:125.
45. Sun R, et al. CBX2 deletion suppresses growth and metastasis of colorectal cancer by Mett13-p38/ERK MAPK signalling pathway. *J Cancer.* 2024;15:2123–36.
46. Wang S, et al. A potent, selective CBX2 chromodomain ligand and its cellular activity during prostate cancer neuroendocrine differentiation. *ChemBioChem.* 2021;22:2335–44.

Publisher's Note

Springer Nature remains neutral with regard to jurisdictional claims in published maps and institutional affiliations.